

The use of RFID technology to measure the compositions of diethyl ether-oil-brine mixtures in enhanced imbibition experiments

Hassan, Anas; Bruining, Hans; Musa, Tagwa; Chahardowli, Mohammad

DOI

[10.1016/j.petrol.2017.06.051](https://doi.org/10.1016/j.petrol.2017.06.051)

Publication date

2017

Document Version

Accepted author manuscript

Published in

Journal of Petroleum Science and Engineering

Citation (APA)

Hassan, A., Bruining, H., Musa, T., & Chahardowli, M. (2017). The use of RFID technology to measure the compositions of diethyl ether-oil-brine mixtures in enhanced imbibition experiments. *Journal of Petroleum Science and Engineering*, 156, 769-779. <https://doi.org/10.1016/j.petrol.2017.06.051>

Important note

To cite this publication, please use the final published version (if applicable). Please check the document version above.

Copyright

Other than for strictly personal use, it is not permitted to download, forward or distribute the text or part of it, without the consent of the author(s) and/or copyright holder(s), unless the work is under an open content license such as Creative Commons.

Takedown policy

Please contact us and provide details if you believe this document breaches copyrights. We will remove access to the work immediately and investigate your claim.

The use of RFID technology to measure the compositions of diethyl ether-oil-brine mixtures in enhanced imbibition experiments

Anas Hassan ^{*}, Hans Bruining [†], Tagwa Musa [‡], Mohammad Chahardowli [§]

June 10, 2017

1 Abstract

Recent developments in Radio Frequency (800MHz-1000MHz) Identification (RFID) devices suggest that it is possible to use them for wireless laboratory measurements of the dielectric coefficients (or compositions) of fluid mixtures with possible spin-off for their use in the petroleum engineering practice. The advantage of RFID devices is their small size ($0.095 \times 0.008 \times 0.001\text{m}^3$), the developments to make them increasingly smaller and that they do not require the use of leak prone connecting cables. RFID measures the response of a sample volume of interest irradiated by a radio frequency electromagnetic (EM) wave. The response can be expressed in terms of various response functions, e.g. two scattering functions (S_{11} and S_{21}) or the minimum irradiated power (P_{min}). The response functions can be measured using a state-of-the-art RFID device (CISC RFID Xplorer-200), which operates in the range between 800-1000 MHz. The effect of the dielectric coefficient on the RFID response was tested by placing the RFID tag in different media with various dielectric coefficients ϵ ranging from 1 to 80. The overall purpose is to develop a work-flow to relate the response functions obtained with RFID technology to the dielectric coefficient and thus the composition of fluid mixtures in which an RFID tag can be immersed. An application is to measure fluid compositions during a spontaneous imbibition experiment in an Amott-cell. As an intermediate step we measure the composition dependence of the partial molar volume of diethyl ether (DEE) in brine and the partial molar volume of DEE in oil by using an Anton Paar density meter. The relation between the dielectric coefficients and the volume fraction can be obtained with the Böttcher mixing rule. The DEE volume fraction range of interest is 0-8 % volume fraction in the aqueous solution whereas DEE volume

^{*}TU Delft, Civil Engineering and Geosciences, and Sudan University of Science and Technology SUST, College of Petroleum Engineering and Technology. E-mail: A.M.Hassan@tudelft.nl

[†]TU Delft, Civil Engineering and Geosciences, Stevinweg 1, 2628 CE Delft, The Netherlands. E-mail: J.Bruining@tudelft.nl

[‡]SUST, Sudan University of Science and Technology, College of Petroleum Engineering and Technology, Khartoum, Sudan. E-mail: tagwamusa@sustech.edu

[§]Sahand University of Technology, Petroleum Engineering, Sahand new town, Tabriz, Iran. E-mail: chahardowli@sut.ac.ir

fraction range of interest is 0-100 % volume fraction in oleic solutions. For better understanding of the measurement results, we used COMSOLTM simulations, which show that the response functions depend on the dielectric coefficient in a vessel of appropriate dimensions filled with a fluid of choice. The measurements show that the minimum power at the tag position P_{min} is the preferred response function and that the sensitivity of P_{min} was highest at 915 and 868 MHz for aqueous (8.547×10^{-6}) and oleic (1.905×10^{-4}) solutions respectively. The measurement error is of the same order of magnitude as the errors mentioned above (Hon, 1989) ensuing from evaporation of DEE during the preparation of the calibration fluids or the approximate nature of the Böttcher mixing rule. We conclude that it is possible to use RFID technology for contact-less measurements of the compositions of fluids in imbibition experiments.

Keywords: Amott-cell; Dielectric coefficient; Laboratory measurement; In-situ fluid composition; Radio Frequency Identification (RFID); Solvent enhanced oil recovery.

2 Introduction

Naturally fractured reservoirs contain around 20% of the world oil reserves ((Salimi, Bruining, et al., 2010a),(Salimi, Bruining, et al., 2010b),(Firoozabadi et al., 2000),(Saidi et al., 1983)). Oil recovery from fractured reservoirs is generally low due to preferential flow in the fractures thus bypassing the oil in the matrix layers ((Hirasaki, Zhang, et al., 2004),(Kleppe, Morse, et al., 1974),(Warren, Root, et al., 1963),(Mattax, KYTE, et al., 1962),(Holm, Cszasz, et al., 1962)), unless water imbibes in the matrix thus expelling oil to the fracture ((Salimi et al., 2010a),(Salimi et al., 2010b)). This mechanism only occurs when the matrix is water wet or made water wet ((Al-Hadhrami, Blunt, et al., 2000),(Motealleh, de Zwart, & Bruining, 2005)). These transfer mechanisms can be conveniently studied in the laboratory by using an Amott-cell. Generally, an Amott-cell is a powerful tool to study processes in fractured reservoirs in the laboratory. The Amott-cell consists of a glass jar with a graded cylinder on the top; the jar contains an oil saturated core, representing the porous medium (matrix) outside the fractures, whereas the fluid surrounding the core represents the fracture (see Figure 1). Experiments in Amott-cells can be used to elucidate mechanisms that can enhance or deteriorate the feasibility of using solvents for improved oil recovery in fractured reservoirs ((Chahardowli et al., 2016),(Chahardowli, Zholdybayeva, Farajzadeh, Bruining, et al., 2013),(Kahrobaei, Farajzadeh, Suicmez, & Bruining, 2012),(Mattax et al., 1962),(Holm et al., 1962)). The most important experimental data comprise in-situ determination of the composition of the fluid mixtures.

There is recent interest to improve the oil recovery in fractured reservoirs using solvents that are mutually soluble in demineralized water or brine solutions and oil ((Parsons et al., 2016),(Chahardowli, 2016),(Chahardowli et al., 2016),(Chernetsky et al., 2015)). Solvent-based oil recovery, which we abbreviate as SEOR, is a process whereby a solvent is injected into an oil reservoir in order to increase the macroscopic and microscopic displacement efficiency, due to a number of mechanisms such as oil swelling, oil density reduction, oil viscosity reduction and wettability alteration ((Chernetsky et al., 2015),(Chahardowli et al., 2013)(Zhou, Morrow, Ma, et al., 2000),(Standal, Haavik, Blokhuis, & Skauge, 1999),(Morrow et al., 1990)). However, due to the high costs of solvents, SEOR only becomes economically viable when the oil price is high and the amount of solvent to be used can be kept low or retrieved. Using minimal amounts of solvent is not only economically attractive but also enhances the effectiveness of the production process ((Govind, Das, Srinivasan, Wheeler, et



Figure 1: Amott-cell Experiment: the Amott-cell contains an oil saturated core, which represents the matrix (porous medium) outside the fractures, and the fluid surrounding the core which represents the fracture.

al., 2008),(Gupta, Gittins, et al., 2007)). Moreover, minimizing the quantity of injected solvent would reduce the environmental impact of SEOR. It would therefore be useful to accurately monitor solvent concentrations in real-time from within the reservoir. This is where R(adio) F(requency) ID(entification) or RFID technology could potentially play an interesting role ((Hassan, 2016), (Laheurte, Ripoll, Paret, & Loussert, 2014),(Liu, Bolic, Nayak, & Stojmenovic, 2008),(Zhang & Wang, 2006)).

The RFID system comprises of a reader that contains both a transmitting antenna, a receiving antenna and a passive tag, which can modulate the signal before transmitting it back to the reader receiver (Want, 2006) (Dobkin, 2012). We use a state of the art RFID set-up (RFID CISC Xplorer200), to measure the response functions as a function of frequency (800 MHz- 1 GHz) and dielectric coefficient, in which the tag is immersed. RFID has attracted considerable interest and is widely used in a number of applications, including supply chain management, public transportation, asset tracking, access control, health care, food industry etc. ((Laheurte et al., 2014),(Dobkin, 2012),(Want, 2006),(Dobkin & Wandinger, 2005),(Cho, Song, Kim, Kim, & Yoo, 2005)). In recent years, the combination of RFID technology with sensory systems has extended its applications to measure a wide range of environmental parameters including temperature ((Law, Bermak, & Luong, 2010),(Vaz et al., 2010),(Shenghua & Nanjian, 2007)), pressure ((DeHennis & Wise, 2002),(Mori, Suemasu, Noguchi, & Sato, 2004),(Beriaín, Rebollo, Fernandez, Sevillano, & Berenguer, 2012),(Opasjumruskit et al., 2006)), humidity ((Amin, Bhuiyan, Karmakar, & Winther-Jensen, 2014),(Virtanen, Ukkonen, Bjorninen, Elsherbeni, & Sydänheimo, 2011),(Virtanen, Ukkonen, Björninen, & Sydänheimo, 2010),(Jia, Heiß, Fu, & Gay, 2008)) and chemical composition ((Fiddes & Yan, 2013),(Potyrailo et al., 2012)).

RFID tags have benefited from innovative research. Novak in his thesis (Novak, 2009) describes the use of the RFID tag as a chemical sensor for trace substances in the liquid phase. Ong et al. (Ong, Grimes, Robbins, & Singh, 2001) show that RFID is capable of monitoring the complex permittivity, i.e. the real and imaginary part of the dielectric coefficient of the medium surrounding the tag. Grimes et al. (Grimes et al., 2002) give an overview of sensors based on remote resonance frequency detection that allow the measurement of a variety of physical parameters. Only very recently the possibility of using RFID for determining dielectric coefficients, has been worked out by Humberto Lobato-Morales et al. ((Lobato-Morales, Corona-Chávez, & Olvera-Cervantes, 2013),(Lobato-Morales et al., 2011)), who use a Substrate-Integrated-Waveguide (SIW) resonant cavity and a tunnel sensor, which allows the determination of the complex permittivity. The dielectric coefficient also depends on the frequency; measurements at various frequencies therefore expand the capability using RFID's for measuring quantities that depend on more than two parameters ((Warnagiris, 2000)). Karappuswami et al. (Karappuswami, Kaur, Ghazali, & Chahal, 2016) is recently published and describe different sensor designs for measurement of dielectric properties via the response functions under far field conditions. Even if the focus of their paper is largely on optimal sensor design but they also report possible applications to fluid compositions, i.e. isopropyl alcohol-water and methanol-water mixtures. Karappuswami's research, which has been carried out in parallel with our research shows overlap with the results described in this paper. However, in addition to (Karappuswami et al., 2016), we explore

the possibility of using RFID technology and its optimization in a laboratory set-up (Amott-cell) (see Figure 2). As a consequence we developed a work-flow including the procedure to relate the composition in terms of volume fraction to the RFID response function with an emphasis on the minimum power at the tag position (P_{min}), which is defined as the minimum power that the passive tag requires in order to be activated.

The work-flow can serve as a template for implementing RFID technology in laboratory experiments, and therefore, e.g. be used to enhance the interpretation capabilities in Amott-cells. This can be accomplished by using the RFID tag to measure the dielectric coefficients of the medium surrounding the tag. This requires the calibration curves of the response functions versus the volume fraction both in the aqueous brine phase and oleic phase; the DEE volume fraction can be conveniently expressed in terms of the partial molar volumes and the mole fractions of the constituents; the use of partial molar volumes results in more linear relationships. Conversely the volume fractions can be used to estimate the dielectric coefficients of the mixtures as a function of the composition using the Böttcher mixing rule. Thus the relation between the response functions and the dielectric coefficients can be determined. However, due to the low boiling point of Diethyl Ether (DEE), a special experimental procedure is necessary, which is therefore described in a separate section devoted to experimental aspects to obtain the calibration curves. For the optimal development of the workflow it is helpful to use COMSOL to simulate the behavior of the RFID system in terms of the RFID response functions to facilitate the interpretation of the measurements. Yeoman and Neill (Yeoman et al., 2009) have developed and implemented a prototype numerical model in COMSOL to obtain the electric field of an RFID system that contains a meandering dipole tag antenna. We modified the Yeoman-Neill model to implement the tag geometry used by us, and used two reader antennae, instead of one. The computed electric field allows to obtain quantities that can be measured by the reader, e.g. the scattering function as a function of frequency. The COMSOL model of Yeoman and Neill does not include modulation of the tag back-scattered signal, so that only the total electric field can be obtained. The model shows that the response mainly depends on the embedding extending several centimeters around the tag (up to 0.03 m). Beyond 0.03 m the response function becomes independent of the size of the embedding.

The organization of the paper is as follows: In section 4 we determine the maximum full solubility of DEE in demineralized water (or brine with zero salt concentration), in brine (0.05M NaCl and 0.5M NaCl) and hexadecane. We establish the calibration curve by using the Anton Paar density meter, using hexadecane-DEE mixtures, brine-DEE mixtures and water-DEE mixtures. From this the partition coefficient as function of the composition is determined. The density meter measurements can be used to determine the partial molar volumes of the constituents as a function of the DEE mole fraction. We use the IDAX-300 Insulation diagnostic system and the Wayne Kerr Precision-6640A to determine the dielectric coefficient of pure hexadecane and DEE and the dielectric coefficient of demineralized water and the brine respectively. Moreover, we apply the Böttcher mixing rule to determine the dielectric coefficient of the brine-DEE and hexadecane-DEE mixtures, using the dielectric coefficients of the pure components and the partial molar volumes. Section 5 has two subsections. In subsection 5.1 we describe the COMSOL simulation. We define the

RFID response functions and give the model equation description. Subsection 5.2 shows the result of the numerical calculations. Section 6 gives an overview of the RFID experiments. Subsection 6.1 describes the RFID set-up. Subsection 6.2 and 6.3 discuss the experimental measurements and results respectively. We end with some conclusions in section 7.

3 Motivation

In order to illustrate why measurements with RFID technology are useful for solvent enhanced imbibition experiments, we consider the following mechanism. When a core is immersed in an Amott cell filled with brine saturated with DEE, imbibition of the aqueous phase into the core occurs while displacing oil to the aqueous phase (see right part of Figure 2). It can be expected that the equilibrium concentration of DEE in the oleic phase is much larger than the DEE concentration in the aqueous phase. As a result, it is inferred that the aqueous layer around the core is quickly scavenged from DEE by oil droplets, which are collected in the graded cylinder of the Amott-cell. With an RFID tag we would be able to validate this mechanism by monitoring the DEE concentration in the aqueous phase surrounding the core and the DEE concentration in the graded cylinder of the Amott cell. If the proposed mechanism would be correct we expect that the DEE concentration in the fluid (oleic phase) collected in the lower part of the graded cylinder quickly reduces to zero. Consequently it is asserted that an RFID tag can be used in an Amott-cell to study the effect of partitioning of DEE concentration in the aqueous and the oleic phase on the efficiency of solvent enhanced imbibition experiments ((Hassan, 2016),(Chahardowli et al., 2016),(Chahardowli et al., 2013)). RFID tags become increasingly smaller, which gives additional possibilities (see left part of Figure.2)

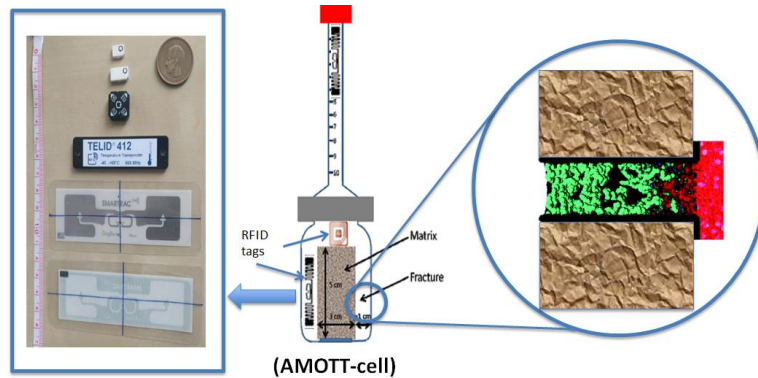


Figure 2: Right part of figure (6) shows counter-current imbibition: the space surrounding the oil saturated core, which is filled with DEE saturated brine (colored red) represents the fracture . The DEE saturated brine penetrates into the core by capillary imbibition from the sides and from the bottom by gravity displacement of the oil (green). In counter-current imbibition flow, the oil and DEE saturated brine flow in opposite directions. Left part of figure (6) shows how RFID tags become increasingly smaller, which makes RFID technology more useful for laboratory and field fluid composition measurements

To clarify the use of small RFID tags, we have added a COMSOL simulation result (Chahardowli et al., 2016) of imbibition and gravity displacement of DEE saturated brine. This occurs when a core is immersed in an aqueous phase with dissolved DEE. Indeed, we observe that the imbibition is combined with gravity displacement from below. An interpretation would consist of an RFID measurement aided with such a simulation. We can anticipate that the oleic phase and aqueous phase leaving at the top contains only small amounts of DEE. By mounting small RFID tags at the top of the core we expect that this effect can be monitored. In summary, by combining RFID measurements with COMSOL simulations, the AMOTT-cell becomes a powerful tool to elucidate relevant details of solvent imbibition and gravity displacement in fractured media.

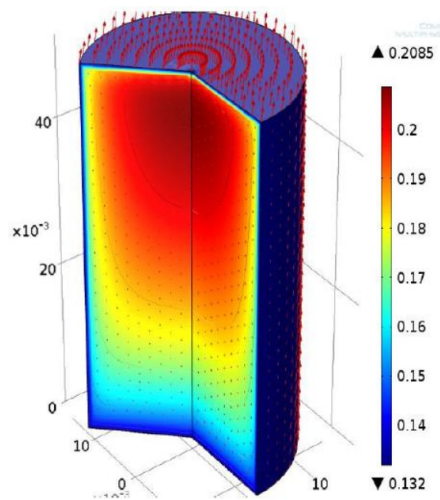


Figure 3: COMSOL simulation of imbibition of brine saturated with DEE into a core filled with oil at connate water saturation. We observe that recovery is partly due to gravity effects and counter-current imbibition. The produced oil will be expelled to the annular space surrounding the core in which RFID tag can be placed. Subsequently, the produced oil will be collected in the graded cylinder on the top of the Amott-cell. The hydrocarbon distribution is shown at about 52.5 days.

4 Phase Behavior

This section describes the behavior of phases in a system of diethyl ether-brine-oil in terms of the partition coefficient of diethyl ether (DEE) between the oleic and the aqueous phase. Moreover, we determine the dielectric coefficients of the mixtures in terms of the pure dielectric coefficients of the pure substances and the volume fraction of DEE ((Hassan, 2016),(Chahardowli, 2016)).

4.1 Measurements of partial molar volume

The purpose of the measurements described here was to obtain an experimental relation between the partial molar volumes of the oleic phase and aqueous phase versus the mole fraction, which can be determined by measuring mass densities with the Anton Paar DMA-4100M density meter (see Figure 4B). The accuracy and precision (see, however,(Hon, 1989)) of the density is 0.0001 g/cm^3 and 0.00005 g/cm^3 respectively. The accuracy and precision of the temperature is $0.05 \text{ }^\circ\text{C}$ and $0.02 \text{ }^\circ\text{C}$ respectively. The cell of the density meter is filled with binary DEE-water mixtures and binary DEE-hexadecane mixtures. The experiments were performed at $23 \text{ }^\circ\text{C}$ and 1 atm. First, the pure solvent (water or hexadecane) was placed in a chemically resistant sample tube and weighed (accuracy 10^{-4} gram) to determine the initial volume. To the weighed sample tube filled with solutions of DEE-water or DEE-hexadecane weighed amounts of DEE were added to obtain aqueous solutions of approximately 0.5-6.5 DEE % wight fraction with increments of 0.5 % weight fraction and oleic solutions of 0.0-25 DEE % weight fraction with increments of about 5 % weight fraction. Using the molecular weight of DEE and water, the compositions of the solutions were converted into mole fractions. As DEE is volatile and can evaporate easily (boiling point at $34 \text{ }^\circ\text{C}$), we use a metal syringe, which is filled both with water or oil from a glass tube and with DEE from a glass jar through a septum. To minimize evaporation we implemented refrigeration using an ice container. To validate negligible evaporation we compared the mass decrease from the glass vessels to the mass increase of the filled syringe (see Figure 4A). The estimated evaporation was measured to be below 10^{-4} gram for a sample volume of at least a milliliter.

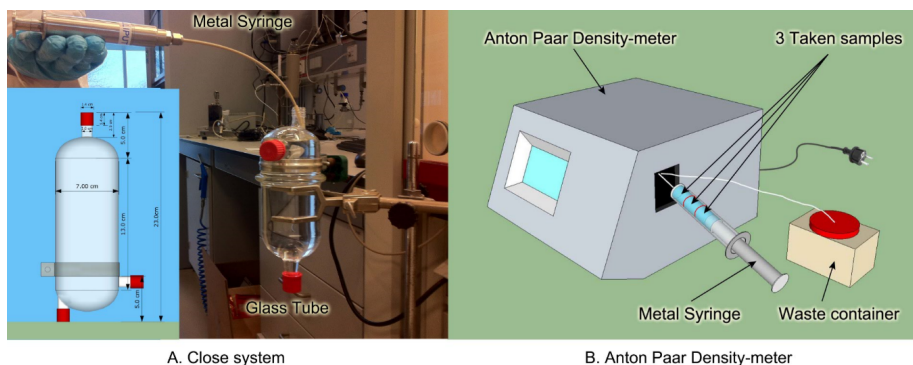


Figure 4: Closed-system and establishing calibration curves using Anton Paar density-meter

The Anton Paar DMA-4100M density meter measures the mass densities $\rho_{\alpha,j}$, in our case, of the DEE-hexadecane mixtures (oleic phase) and the DEE-water and the DEE-brine mixtures of known molar fractions. Using the molar fraction it is possible to obtain the mole fraction averaged molecular weight M_{av} . Division of the mass density by average mole fraction averaged molecular weight leads to the molar density $\rho_{mol,\alpha,j} = \rho_{\alpha,j}/M_{av}$ (Smith, Van Ness, & Abbott, 1987). The partial molar volume of pure water is $\nu_{w,H_2O} = 18.0622$ and of hexadecane $\nu_{o,HEX} = 293.44$. By plotting the inverse molar density versus mole fraction it is possible to obtain the partial molar volume (inverse molar density) as a function of the mole fraction. Figure 5A shows the partial molar volume of the DEE-hexadecane mixture versus the composition expressed in mole fraction. It is approximately a straight-line. The straight-line indicates that the partial molar volumes of the constituents in the mixture, i.e. the partial molar volume of DEE and hexadecane are more or less independent of the composition (Smith et al., 1987). Figure 5B shows the partial molar volume of demineralized water-DEE mixtures and salt solutions mixtures, which are also approximately independent of the composition.

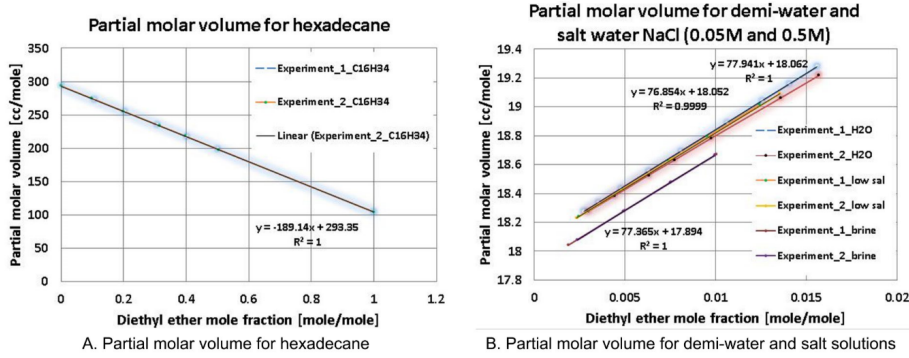


Figure 5: Partial molar volume calibration curves for oleic and aqueous phase

Extrapolation to mole fractions of one in Figure 5A and Figure 5B shows that the partial molar volume of DEE in water is $\nu_{w,DEE} = 94.906 \text{ cm}^3/\text{mole}$ and the molar volume of DEE in hexadecane $\nu_{o,DEE} = 104.21 \text{ cm}^3/\text{mole}$. Indeed the partial molar volume of DEE in water is usually smaller than in organic solvents (Israelachvili, 2011). For the ease of reference we have summarized the coefficients a and b in Table 1.

Table 1: The coefficients of the linear regression between the partial molar volume and the mole fraction of DEE ($v = ax + b$)

Component	Coefficient (a)	Coefficient (b)
C16H34-exp1	-189.08	293.29
C16H34-exp2	-189.14	293.35
H2O-exp1	77.914	18.062
H2O-exp2	72.064	18.057
NaCl (0.05M)-exp1	77.687	18.052
NaCl (0.05M)-exp2	76.854	18.052
NaCl (0.5M)-exp1	76.988	17.899
NaCl (0.5M)-exp2	77.365	17.594

After obtaining the experimental relation between the partial molar volumes of the oleic phase and aqueous phase versus the mole fraction, we determine the partition coefficient of DEE between the oleic and aqueous phase by calculating the solvent concentration in the oleic and aqueous phase from previously established calibration curves (Hassan, 2016). The partition coefficient is the ratio of the DEE concentration (or DEE volume fraction) in the oleic phase divided by the DEE concentration (or DEE volume fraction) in the aqueous phase. Figure 6 shows the partitions coefficients of DEE between the Oleic and aqueous (demineralized water-DEE mixtures and salt solutions mixtures) phase as function of the composition.

Furthermore, we use the volume fraction $v_{\alpha,i}$ of the components i in phase α and the pure component dielectric coefficients ε_i to calculate the dielectric coefficient of mixtures ε_m by applying the Böttcher mixing rule

$$\frac{\varepsilon_1 - \varepsilon_m}{\varepsilon_1 + 2\varepsilon_m}v_{\alpha,1} + \frac{\varepsilon_2 - \varepsilon_m}{\varepsilon_2 + 2\varepsilon_m}v_{\alpha,2} = 0 \quad (1)$$

where the volume fraction of component j in phase α , i.e. $v_{\alpha,j}$ is given by

$$v_{\alpha,j} = \frac{x_j v_{\alpha,j}}{x_j v_{\alpha,j} + (1 - x_j) v_{\alpha,k \neq j}}, \quad (2)$$

and where x_j is the mole fraction of component j . As pure components we selected demineralized water (brine with zero salt concentration) ($\varepsilon_w = 79.08$), hexadecane ($\varepsilon_h = 2.05$) and DEE ($\varepsilon_D = 4.24$) at 23 ± 0.02 °C. We measure the dielectric coefficients of the pure substances using the IDAX-300 Insulation diagnostic system and the Wayne Kerr Precision-6640A. The thus obtained experimental values can be compared with tabulated values in the literature. For water ($\varepsilon_w = 79.19$), for hexadecane ($\varepsilon_h = 2.049$), and for DEE ($\varepsilon_D = 4.43$). (Wille, Buggert, Mokrushina, Arlt, & Smirnova, 2010)(Predel, 2006)(Wohlfarth,

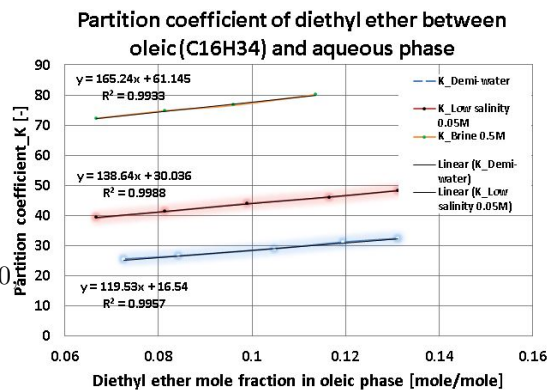


Figure 6: Partition coefficients as function of the composition.

2008)(Wyman Jr, 1933) Figure 7 plots the dielectric coefficient on logarithmic scale versus the molar volume fraction. We use the logarithmic scale to clearly show the behavior of both the DEE-Water mixture and DEE-Oil mixture in a single plot. The dielectric coefficient of the DEE-water mixture is approximately linear in the molar volume fraction range of interest (0-8 % volume fraction). The Dielectric coefficient of the DEE-Oil mixture is approximately linear over the entire range (0-100 % volume fraction).

5 COMSOL Simulation

The work described here follows the paper of Yeoman and Neill (Yeoman et al., 2009) and their implementation in COMSOLTM. In the COMSOL program we adapt the configuration of the antennae and the detailed configuration of the tag (RFID device) to correspond to the outlay used by us. The geometrical outlay of the setup used by us consists of two reader antennae (emitting and receiving) and a passive tag. The reader antennae are at a distance of 10.0 *cm* from each other (edge to edge), where the emitting antenna (Tx) coincides with the *xz*-plane and the receiving antenna (Rx) is rotated (45°) around the *z*-axis counter clock wise. The tag (port-2) is located at a distance of 0.5 *m* from the emitting antenna (port-1), and the Tx and the Rx reader antennae are at a distance of 10 *cm* from each other (see Figure 8). The tag that we used in the experiment is shown in Figure 12 and 13.

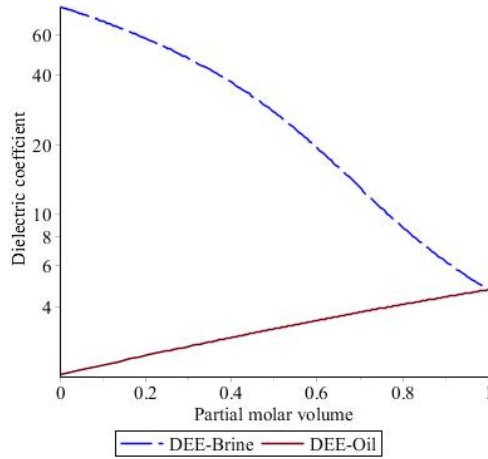


Figure 7: Dielectric coefficient versus Diethyl ether (DEE) volume fraction in oleic and aqueous phase.

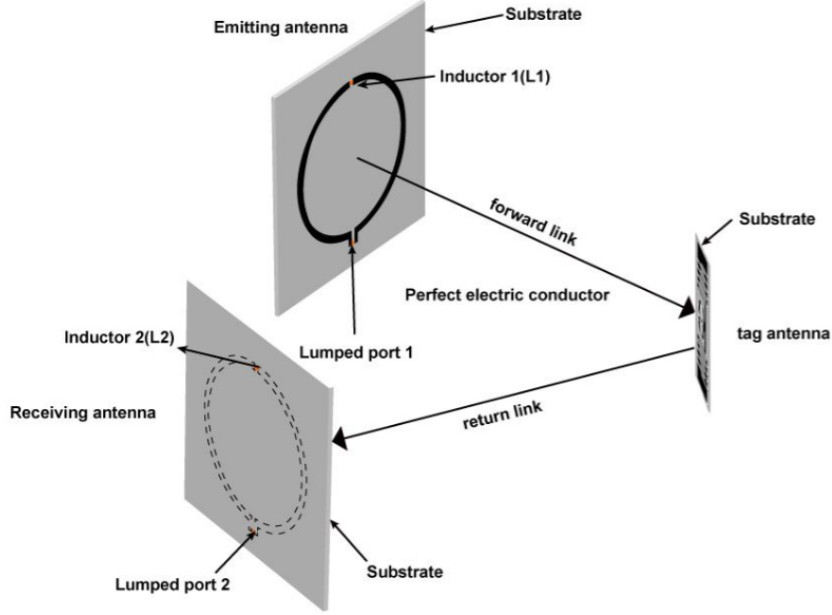


Figure 8: COMSOL simulation model: the Tx antenna parallel and at 0.2 m from the Rx antenna. The tag is placed parallel at 0.5 m distance from both antennae.

5.1 Theory and model equation

The Maxwell equation that describes the electric field \mathbf{E} in the entire domain is

$$\nabla \times \mu_r^{-1} (\nabla \times \mathbf{E}) - \left(\frac{\omega}{c}\right)^2 \left(\varepsilon_r - \frac{j\sigma}{\omega\varepsilon_0}\right) \mathbf{E} = 0, \quad (3)$$

where $\mu_r = 1$ is the relative magnetic permeability, ω is the angular frequency, c is the velocity of light, ε is the dielectric coefficient, and σ is the conductivity. In the COMSOL simulation, we consider a spherical domain filled with air bounded by a conducting sphere with boundary condition $\nabla \times \mathbf{E} = 0$. We can say that the sphere of air is bounded by a perfectly matched layer (PML), which excludes all EM disturbances coming from outside the sphere. In the domain we have Tx and Rx reader antennae, which consist of two parallel Teflon plates ($10\text{cm} \times 10\text{cm}$) with two half circular conductors. The two half circles are closed on the top with lumped inductances of 66 nH . The emitting antenna of the reader is put at one volt. The reader antennae have both an impedance of $50\ \Omega$ whereas the impedance of the tag is $11+143j\ \Omega$. We solve Eq.(3) subject to the boundary conditions (PML of the outer sphere and the voltages applied on the antennae) to obtain the electric field in the entire domain (see Figure 9). For our configuration all arrows are of equal length thus the figure shows only the direction of the electric field vector. The electric field is the gradient of the potential ($\mathbf{E} = -\nabla V$). From the electric field \mathbf{E} we can calculate the response functions, e.g. Scattered functions S_{21} , which are related to the minimum power

at the tag position (P_{min}), to be obtained experimentally in section 6. The S_{12} function is defined as the logarithm (see Eq.(4) and Eq.(5)) of the voltage ratio between the input V_2 at port-2 and the output V_1 also at port-1 (Dobkin, 2012), i.e.

$$S_{21} =^{10} \log \frac{V_2}{V_1} [dB]. \quad (4)$$

The S_{11} parameter is defined by the voltage ratio between the input V_1 at port-1 and the output V_1 also at port-1 (Dobkin, 2012)

$$S_{11} =^{10} \log \frac{V_1}{V_1} [dB]. \quad (5)$$

We use the computed response functions S_{11} and S_{21} as function of the frequency as output of the numerical code. Note that the model of Yeoman and Neill, show the response functions S_{11} and S_{21} in vacuo, whereas our simulations show the response functions S_{11} and S_{21} for a tag embedded in a medium with dielectric coefficient $\varepsilon > 1$. The purpose of the COMSOL simulation is to show that the effect of the dielectric coefficient of the medium on the response functions is significant. The numerical simulations indicate that the output of the RFID system can be used to determine the dielectric coefficient of the medium in which the tag is immersed.

5.2 COMSOL Results

The main results of the COMSOL simulation are the scattering functions S_{11} and S_{21} in the frequency range of (800-1000 MHz). Figure 10A shows the response function S_{11} as function of frequency between 800 MHz-2.5 GHz for the base case and for various dielectric coefficients between 1-80 as indicated in the insert. We observe that the response function S_{11} is insensitive to the dielectric coefficient. Figure 10B shows the response function S_{21} as function of frequency between 800 MHz-2.5 GHz for the base case and for various dielectric coefficients between 1-80 as indicated in the insert. We observe that the response function S_{21} significantly depends on the value of the dielectric coefficient. The wave like structure of S_{21} shifts to the left for increasing dielectric coefficient except for water where it shifts to the right. Figure 11A shows the response function S_{11} as function of the frequency between 800 MHz-2.5 GHz for the base case, and for various dielectric coefficients between 1-80 as indicated in the insert. We observe that the response function S_{11} is insensitive to the volume of the box in which the tag is encased.

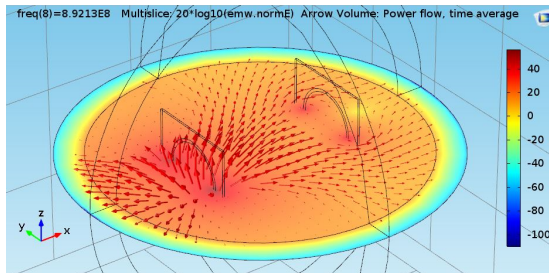


Figure 9: electric field vector shows the normalized electric field in dB ($^{20} \log_{10} E_2 / E_{ref}$) in a color graph in the $z = 0$ plane. Moreover it shows with arrows the direction of the electric field. The highest values of the normlized electric field occur near the emitting antenna

Figure 11B shows the S_{21} response function as a function of frequency for various thicknesses of the dielectric box. In the wave like structure, we observe that the amplitude of the wave slightly decreases with increasing thickness until it reaches a thickness of 3 cm beyond which the results stay more or less constant. Moreover, the Teflon chemical protection bag (0.06 mm) in which the RFID tag was wrapped had only negligible influence on the measurements. We conclude that the response function S_{21} is the preferred response function, which is not much affected by the the thickness of the encasement, but is sensitive to the dielectric coefficient.

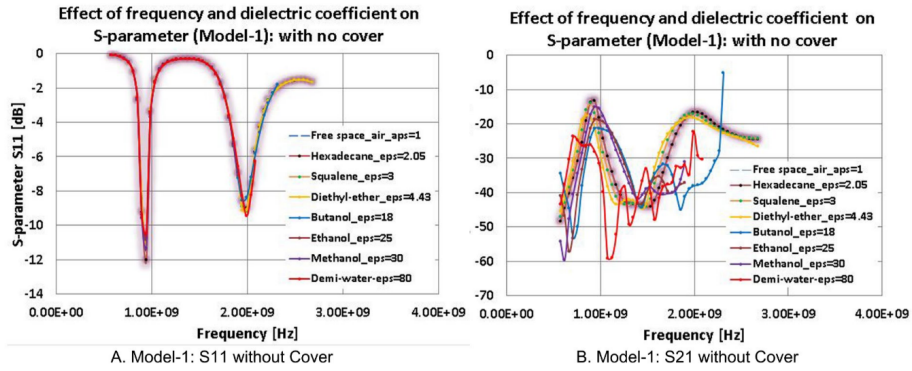


Figure 10: The effect of dielectric coefficient on S_{11} and S_{21}

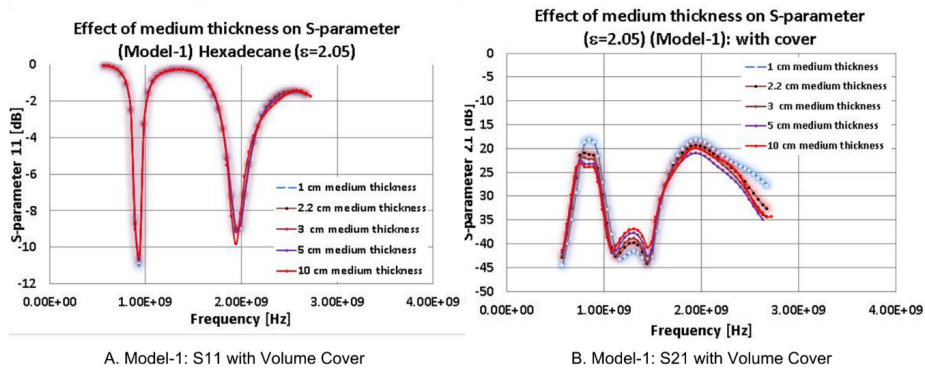


Figure 11: The effect of medium thickness on S_{11} and S_{21}

6 RFID Experiment

6.1 RFID set-up

The RFID set-up consists of a transmitting (Tx) antenna, a receiving (Rx) antenna and the passive tag. The tag is the same as described for the COMSOL simulation and configured as described below (see Figure 12). The transmitting and the receiving antennae are separate entities. Separate transmitting and receiving antennae allow to optimally separate the incident and backscattered power measurements. In this setup, the Tx antenna emits Left-Hand Circularly Polarized (LHCP) radiation and the Rx antenna receives Right-Hand Circularly Polarized (RHCP) radiation (see Figure 12). As shown in Figure 13, the Tx and Rx antennae are mounted on a square plastic cover of size $20 \times 20 \times 0.2 \text{ cm}^3$ with a constant dielectric coefficient ($\epsilon = 2.1$). The covers are placed perpendicular to the $z = 0$ plane. The antennae consist of a copper circular ring with a radius of 10 cm and a thickness of 1 mm in the same way as described for the COMSOL simulation above. The z -coordinate of the midpoint of the tag coincides with the z -coordinate of the midpoint of the covers. The line connecting the midpoints of the tag and the cover of the emitting antenna is perpendicular to the cover-plane. The other cover is rotated 45° around the z -axis (see Figure 13). Both antennae are connected with the reader by a coaxial cable. The distance between the midpoints of the two antennae is 0.2 m and the distance between the emitting antenna and the tag is 0.5 m, which causes that the set-up operates in the far-field domain (Dobkin, 2012). The RFID setup is located far away from the laboratory walls, floor and ceiling such that it is minimally affected by the surrounding environment.

The RFID setup can measure the frequency dependence of two selected response functions in terms of the scattering function S_{21} and in terms of minimum power at the tag position (P_{min}) as a function of the dielectric coefficient. The S_{21} and P_{min} functions are interrelated. We performed a calibration of the frequency dependent RFID response functions as a function of the dielectric coefficient. This is accomplished by immersing the RFID tag in a cylindrical tube, with a diameter of 0.05 m and a height 0.35 m, filled with fluids (till 0.2 m height and a volume of 0.00039 m^3) of various known dielectric coefficients ($\epsilon = [1, 80]$). By plotting the RFID response functions at various frequencies as a function of the

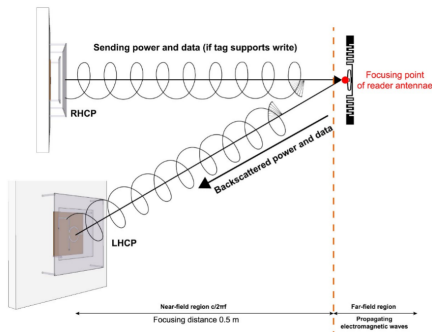


Figure 12: RFID communication system: this experiment use passive tag, which contains no battery, the tag-reader communication process is always initiated by the reader emitting antenna (RHCP), the tag can modulate the signal before transmitting it back to the receiver antenna (LHCP).

dielectric coefficient an optimal frequency can be found for which the dielectric dependence is most sensitive.

6.2 Experimental measurements

The aim of using the RFID set-up is to measure the tag response functions for various media (with dielectric coefficients between 1 and 80). Of the possible response functions, we specifically measured the minimum power at the tag position (P_{min}) and the scattering function, S_{21} . The minimum power at the tag position can be related to the scattered signal at the midpoint of the tag with respect to the input signal at the emitting antenna. The measurements are performed at 23°C in the frequency range between 800-

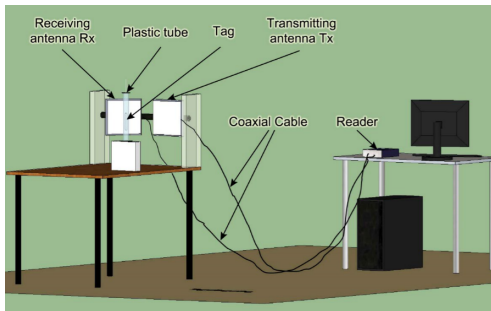


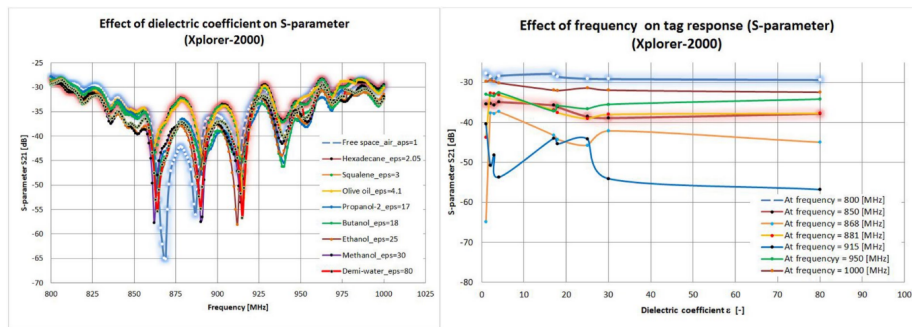
Figure 13: RFID Xplorer setup: the tag is placed in a cylindrical plastic tube filled with different liquids, with varying dielectric coefficient (ϵ between 1-80).

1000 MHz (with frequency steps of 5 MHz). We started our calibration process by measuring in air ($\epsilon = 1$). As the system is designed to operate in air this is considered as our base case. We did not measure other response functions because it turned out that P_{min} gave optimal results. Measurements for other dielectric coefficients were done by placing the tag in a cylindrical (polypropylene, $\epsilon = 2.2$) tube (with an outside diameter of 0.05 m, an inside diameter of 0.046 m and a height of 0.35 m, and filled up to 0.2 m, corresponding to a volume 0.00039 m³). The cylindrical polypropylene tube, which is chemically resistant against the used fluids, is filled with different liquids such as water, oil and alcohol (propanol, butanol, ethanol and methanol) with various dielectric coefficients (between 1-80). The tube (volume of 0.00039m³) is filled up to a height of 0.2m; the top 0.15 m is filled with air. The tag is fully immersed in the liquid.

6.3 Experimental Results and Discussions

This experiment seeks to measure the effect of the dielectric coefficient ϵ on the RFID response functions obtained with the CISC (Xplorer-200) setup. In this study, we determine the response functions S_{21} and P_{min} . The response function S_{21} is equal to $^{10}\log V_2/V_1$ dBm, where V_2 is the voltage measured at port-2 and V_1 is the applied voltage at port-1. The response function P_{min} ($^{10}\log_{10}(V)$ dBm) is the minimum voltage required to activate the RFID tag. Figure 14A shows the S_{21} versus frequency for air $\epsilon \approx 1$, hexadecane $\epsilon = 2.05$, diethyl ether $\epsilon = 4.1$, a variety of alcohols (ethanol with $\epsilon = 25$, methanol $\epsilon = 33$, propanol $\epsilon = 18$, butanol $\epsilon = 17$) mixtures of alcohol and ($\epsilon \in 17 - 33$) and water $\epsilon = 80$. We observe an oscillatory structure for a frequency ranging

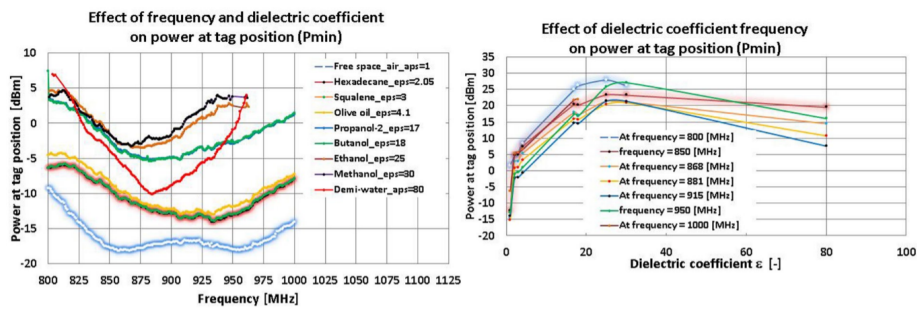
between 800-1000 MHz, with mainly four distinct peaks. The position of the peaks shifts monotonously to the left for increasing dielectric coefficients, except for water where the peaks shift to the right. This is possibly due to a conductivity effect of distilled water brought about by dissolution of carbon dioxide. Figure 14B plots the scattering function S_{21} versus the dielectric coefficient for given frequencies, e.g. 868 MHz, 915 MHz. These frequencies show the highest sensitivity of S_{21} to the dielectric coefficient between diethyl ether-oil and diethyl ether-water respectively. Figure 15A plots the minimum power P_{min} versus the frequency for the same fluids as used for the scattering function S_{21} . P_{min} shows a less oscillatory behavior than S_{21} . The minimum power increases for increasing dielectric coefficient. Between 800-1000 MHz we observe a single minimum around 900 MHz, except for water where we observe two minima at 850 MHz and 950 MHz respectively. We use the data to construct Figure 15B to plot the P_{min} versus the dielectric coefficient for selected frequencies. Again the frequency 868 MHz and 915 MHz shows the highest sensitivity. In Figures 16 and 17 we convert the dielectric coefficient to volume fraction using the Böttcher mixing rule as explained in Section 4. The volume fraction range of DEE of interest is up to 8 % volume fraction. Figure 16A shows the scattering function S_{21} changing only significantly at 950 MHz (sensitivity 124.5 [dBm/ volume fraction%]) and therefore only the behavior at 950 MHz is preferably used to determine the volume fraction of DEE in the aqueous solution. Figure 16B shows the S_{21} response function versus the volume fraction of DEE in the oleic phase. This shows that 850 MHz (sensitivity 13.5 [dBm/ volume fraction %]) and 868 (sensitivity 9.5 [dBm/ volume fraction %]) are the optimal frequencies to determine the fluid composition in the entire range 0-100 % volume fraction. Figure 17A shows the P_{min} as a function of the volume fraction of DEE in the aqueous phase. The volume fraction range of interest is 0 – 8%*volume fraction*, the optimal frequencies are 915 (sensitivity 46.8 [dBm/ volume fraction%]) and 950 (sensitivity 46.4 [dBm/ volume fraction %]) MHz. Figure 17B shows the response function P_{min} as a function of the volume fraction of DEE in the oleic phase. The frequencies, 800 MHz (sensitivity 2.6 [dBm/ volume fraction %]), 850 MHz (sensitivity 2.3 [dBm/ volume fraction %]) and 868 MHz (sensitivity 2.1 [dBm/ volume fraction %]), are optimal to determine the composition in the entire range. The RFID manual states that the accuracy with which the response function can be measured is (0.0004 dBm). By dividing the standard deviation by the sensitivity, we can estimate the precision with which, the composition can be determined. Therefore we conclude that P_{min} is the preferred response function at frequencies of 915 and 950 MHz for the oleic phase and 800, 850 and 868 MHz for the aqueous phase.



A. XplorerS21 with Water (Cover)

B. XplorerS21 vs Dielectric coefficient

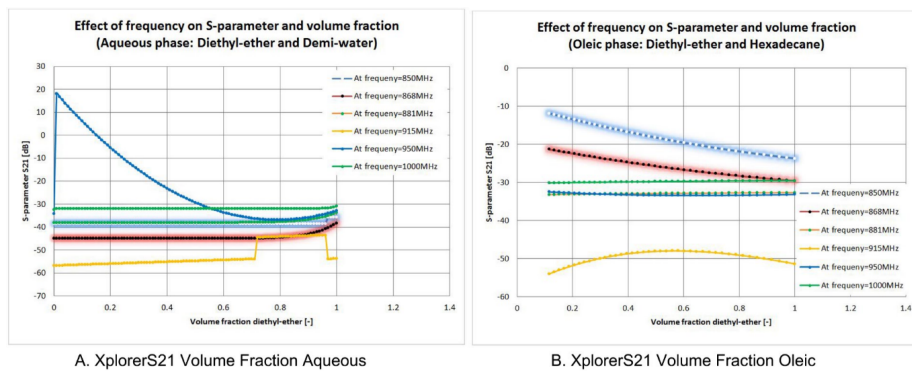
Figure 14: The effect of dielectric coefficient and frequency on S_{21}



A. Xplorer P_{min} vs Frequency (Cover)

B. Xplorer P_{min} Dielectric Coefficient

Figure 15: The effect of dielectric coefficient and frequency on P_{min}



A. XplorerS21 Volume Fraction Aqueous

B. XplorerS21 Volume Fraction Oleic

Figure 16: S_{21} versus volume fraction of DEE in aqueous and oleic phase

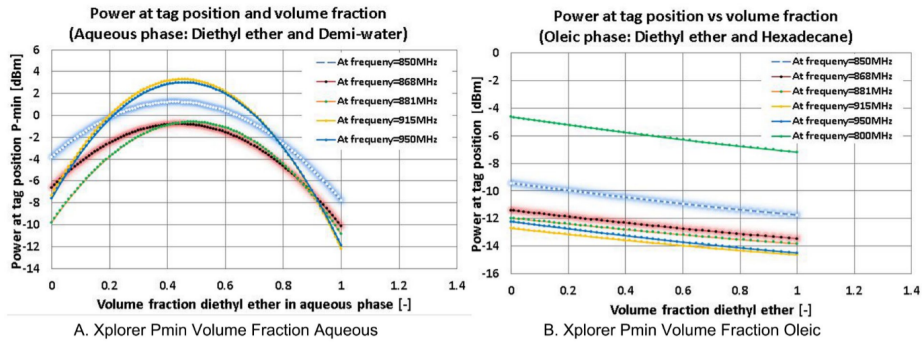


Figure 17: P_{min} versus volume fraction of DEE in aqueous and oleic phase

7 Conclusion

This paper developed a work-flow to relate the response functions (S_{21} and P_{min}) obtained with RFID technology to the dielectric coefficient and thus the composition of a fluid mixtures in which an RFID tag can be immersed. An application is to measure fluid compositions during a spontaneous imbibition experiment in an Amott-cell. Firstly, the work-flow consists of measurements of the partial molar volume of diethyl ether (DEE) in brine and the partial molar volume of DEE in oil by using an Anton Paar density meter. Secondly, we use the Böttcher mixing rule to relate the dielectric coefficient of mixtures to the volume fraction which can be obtained from the partial molar volume and the mole fraction. The DEE volume fraction range of interest is 0-8 % volume fraction in aqueous solutions, whereas the dielectric coefficient is between 79.084-70.214. The DEE concentration range of interest is 0-100 % volume fraction in oleic solutions, where the dielectric coefficient is between 2.049-4.739. For the calibrations it is possible to use alcohol (butanol, propanol, ethanol and methanol)-water mixtures for the aqueous phase whereas for the oleic phase and air ($\epsilon = 1$), hexadecane ($\epsilon = 2.05$), squalene ($\epsilon = 3.0$) and olive oil ($\epsilon = 4.1$) can be used. Thirdly, for better understanding of the measurement results, we used COMSOLTM simulations to (a) show that the Teflon chemical protection bag (0.06 mm) in which the RFID tag was wrapped had only negligible influence on the measurements, (b) to show the effect of the thickness of the box (between 1-10 cm) with given dielectric coefficient ($\epsilon = 2.1$) in which the RFID tag was mounted; beyond 3 cm the response function S_{21} stays unchanged, (c) to show that the response function S_{21} depends on the dielectric coefficient of the box (between 1-80). Fourthly, a CISC RFID setup can be used to measure the response functions (S_{21} and P_{min}) as a function of frequency (800-1000 MHz) and the dielectric coefficient in which RFID was encased. The measurements show that the sensitivity of the minimum power at the tag position P_{min} was highest at 915 and 868 MHz for aqueous (8.547×10^{-6}) and oleic (1.905×10^{-4}) solutions respectively and the error of measurement with the RFID tag is negligible with respect to other errors (Hon, 1989). Therefore, the error due to the evaporation of DEE during the preparation of the calibration fluids is of the same order of magnitude as the error ensuing from the RFID experiments. The measurements

until now, show that it is possible to use RFID technology for contact-less measurements of the compositions of fluids in imbibition experiments.

8 Acknowledgments

The work was supported by Geoscience and Engineering Laboratory of Delft University of Technology (TU Delft). The authors would like to acknowledge Prof. dr. W. R (William) Rossen and Ing. H.K.J. Heller for useful suggestions. Parts of this report greatly benefited from discussions with Prof. ir. Cor van Kruijsdijk and Dr. Christian Schoemaker.

References

- Al-Hadhrami, H. S., Blunt, M. J., et al. (2000). Thermally induced wettability alteration to improve oil recovery in fractured reservoirs. In *Spe/doe improved oil recovery symposium*.
- Amin, E. M., Bhuiyan, M. S., Karmakar, N. C., & Winther-Jensen, B. (2014). Development of a low cost printable chipless rfid humidity sensor. *IEEE Sensors Journal*, *14*(1), 140–149.
- Beriain, A., Rebollo, I., Fernandez, I., Sevillano, J. F., & Berenguer, R. (2012). A passive uhf rfid pressure sensor tag with a 7.27 bit and 5.47 pj capacitive sensor interface. In *Microwave symposium digest (mtt), 2012 ieee mtt-s international* (pp. 1–3).
- Chahardowli, M. (2016). Dimethyl ether & diethyl ether for enhanced oil recovery from conventional & fractured reservoirs. *PhD thesis TU-Delft*, 1–149.
- Chahardowli, M., Farajzadeh, R., Masalmeh, S., Mahani, H., Bruining, H., et al. (2016). A novel enhanced oil recovery technology using dimethyl ether/brine: Spontaneous imbibition in sandstone and carbonate rocks. In *Spe annual technical conference and exhibition*.
- Chahardowli, M., Zholdybayeva, A., Farajzadeh, R., Bruining, H., et al. (2013). Solvent-enhanced spontaneous imbibition in fractured reservoirs. In *Eage annual conference & exhibition incorporating spe europe*.
- Chernetsky, A., Masalmeh, S., Eikmans, D., Boerrigter, P., Fadili, A., Parsons, C., ... others (2015). A novel enhanced oil recovery technique: Experimental results and modelling workflow of the dme enhanced waterflood technology. In *Abu Dhabi international petroleum exhibition and conference*.
- Cho, N., Song, S.-J., Kim, S., Kim, S., & Yoo, H.-J. (2005). A 5.1-/spl mu/w uhf rfid tag chip integrated with sensors for wireless environmental monitoring. In *Solid-state circuits conference, 2005. esscirc 2005. proceedings of the 31st european* (pp. 279–282).
- DeHennis, A., & Wise, K. D. (2002). A double-sided single-chip wireless pressure sensor. In *Micro electro mechanical systems, 2002. the fifteenth ieee international conference on* (pp. 252–255).
- Dobkin, D. M. (2012). *The rf in rfid: Uhf rfid in practice*. Newnes.

- Dobkin, D. M., & Wandinger, T. (2005). A radio oriented introduction to radio frequency identification. *RFID Tutorial, High Frequency Electronics*.
- Fiddes, L. K., & Yan, N. (2013). Rfid tags for wireless electrochemical detection of volatile chemicals. *Sensors and Actuators B: Chemical*, 186, 817–823.
- Firoozabadi, A., et al. (2000). Recovery mechanisms in fractured reservoirs and field performance. *Journal of Canadian Petroleum Technology*, 39(11).
- Govind, P. A., Das, S. K., Srinivasan, S., Wheeler, T. J., et al. (2008). Expanding solvent sagd in heavy oil reservoirs. In *International thermal operations and heavy oil symposium*.
- Grimes, C. A., Mungle, C. S., Zeng, K., Jain, M. K., Dreschel, W. R., Paulose, M., & Ong, K. G. (2002). Wireless magnetoelastic resonance sensors: A critical review. *Sensors*, 2(7), 294–313.
- Gupta, S., Gittins, S., et al. (2007). Effect of solvent sequencing and other enhancements on solvent aided process. *Journal of Canadian Petroleum Technology*, 46(09).
- Hassan, A. (2016). *The use of rfid technology in solvent-enhanced imbibition experiments*. LAP Lambert Academic Publishing. Retrieved from <https://books.google.nl/books?id=2yUqvgAACAAJ>
- Hirasaki, G., Zhang, D. L., et al. (2004). Surface chemistry of oil recovery from fractured, oil-wet, carbonate formations. *Spe Journal*, 9(02), 151–162.
- Holm, L., Csaszar, A., et al. (1962). Oil recovery by solvents mutually soluble in oil and water. *Society of Petroleum Engineers Journal*, 2(02), 129–144.
- Hon, G. (1989). Towards a typology of experimental errors: An epistemological view. *Studies in History and Philosophy of Science Part A*, 20(4), 469–504.
- Israelachvili, J. N. (2011). *Intermolecular and surface forces*. Academic press.
- Jia, Y., Heiß, M., Fu, Q., & Gay, N. A. (2008). A prototype rfid humidity sensor for built environment monitoring. In *Education technology and training, 2008. and 2008 international workshop on geoscience and remote sensing. ett and grs 2008. international workshop on* (Vol. 2, pp. 496–499).
- Kahrobaei, S., Farajzadeh, R., Suicmez, V. S., & Bruining, J. (2012). Gravity-enhanced transfer between fracture and matrix in solvent-based enhanced oil recovery. *Industrial & Engineering Chemistry Research*, 51(44), 14555–14565.
- Karuppuswami, S., Kaur, A., Ghazali, M. I. M., & Chahal, P. (2016). Rfid compatible sensor tags for remote liquid sample interrogation. In *Electronic components and technology conference (ectc), 2016 ieee 66th* (pp. 2401–2407).
- Kleppe, J., Morse, R. A., et al. (1974). Oil production from fractured reservoirs by water displacement. In *Fall meeting of the society of petroleum engineers of aime*.
- Laheurte, J.-M., Ripoll, C., Paret, D., & Loussert, C. (2014). *Uhf rfid technologies for identification and traceability*. John Wiley & Sons.
- Law, M. K., Bermak, A., & Luong, H. C. (2010). A sub- μ mw embedded cmos temperature sensor for rfid food monitoring application. *IEEE journal of solid-state circuits*, 45(6), 1246.
- Liu, H., Bolic, M., Nayak, A., & Stojmenovic, I. (2008). Taxonomy and challenges of the integration of rfid and wireless sensor networks. *IEEE network*, 22(6).

- Lobato-Morales, H., Corona-Chávez, A., & Olvera-Cervantes, J. L. (2013). Planar sensors for rfid wireless complex-dielectric-permittivity sensing of liquids. In *Microwave symposium digest (ims), 2013 ieee mtt-s international* (pp. 1–3).
- Lobato-Morales, H., Murthy, D., Corona-Chávez, A., Olvera-Cervantes, J. L., Martínez-Brito, J., & Guerrero-Ojeda, L. G. (2011). Permittivity measurements at microwave frequencies using epsilon-near-zero (enz) tunnel structure. *IEEE transactions on microwave theory and techniques*, *59*(7), 1863–1868.
- Mattax, C. C., Kyte, J., et al. (1962). Imbibition oil recovery from fractured, water-drive reservoir. *Society of Petroleum Engineers Journal*, *2*(02), 177–184.
- Mori, T., Suemasu, Y., Noguchi, H., & Sato, T. (2004). Multiple people tracking by integrating distributed floor pressure sensors and rfid system. In *Systems, man and cybernetics, 2004 ieee international conference on* (Vol. 6, pp. 5271–5278).
- Morrow, N. R., et al. (1990). Wettability and its effect on oil recovery. *Journal of Petroleum Technology*, *42*(12), 1–476.
- Motealleh, S., de Zwart, B.-R., & Bruining, J. (2005). Wettability alteration and imbibition effects in steam recovery from matrix blocks in fractured reservoirs. In *Ior 2005-13th european symposium on improved oil recovery*.
- Novak, G. D. (2009). *Rfid tags/planar inductors as chemical sensor platforms in liquid sensing applications* (Unpublished doctoral dissertation). MARQUETTE UNIVERSITY.
- Ong, K. G., Grimes, C., Robbins, C., & Singh, R. (2001). Design and application of a wireless, passive, resonant-circuit environmental monitoring sensor. *Sensors and Actuators A: Physical*, *93*(1), 33–43.
- Opasjumruskit, K., Thanhipwan, T., Sathusen, O., Sirinamarattana, P., Gadmanee, P., Pootarapan, E., . . . Thamsirianunt, M. (2006). Self-powered wireless temperature sensors exploit rfid technology. *IEEE Pervasive computing*, *5*(1), 54–61.
- Parsons, C., Chernetsky, A., Eikmans, D., te Riele, P., Boersma, D., Sersic, I., . . . others (2016). Introducing a novel enhanced oil recovery technology. In *Spe improved oil recovery conference*.
- Potyralo, R. A., Nagraj, N., Tang, Z., Mondello, F. J., Surman, C., & Morris, W. (2012). Battery-free radio frequency identification (rfid) sensors for food quality and safety. *Journal of agricultural and food chemistry*, *60*(35), 8535–8543.
- Predel, B. (2006). *Landolt-bornstein, group iv: Physical chemistry*. Springer, Berlin.
- Saidi, A., et al. (1983). Simulation of naturally fractured reservoirs. In *Spe reservoir simulation symposium*.
- Salimi, H., Bruining, J., et al. (2010a). Improved prediction of oil recovery from waterflooded fractured reservoirs using homogenization. *SPE Reservoir Evaluation & Engineering*, *13*(01), 44–55.
- Salimi, H., Bruining, J., et al. (2010b). The influence of wettability on oil recovery from naturally fractured oil reservoirs including non-equilibrium effects. In *Spe latin american and caribbean petroleum engineering conference*.

- Shenghua, Z., & Nanjian, W. (2007). A novel ultra low power temperature sensor for uhf rfid tag chip. In *Solid-state circuits conference, 2007. asscc'07. ieee asian* (pp. 464–467).
- Smith, J., Van Ness, H., & Abbott, M. (1987). Introduction to chemical engineering thermodynamics, ; macgraw hill. *Inc.: New York*.
- Standal, S., Haavik, J., Blokhus, A., & Skauge, A. (1999). Effect of polar organic components on wettability as studied by adsorption and contact angles. *Journal of Petroleum Science and Engineering*, *24*(2), 131–144.
- Vaz, A., Ubarretxena, A., Zalbide, I., Pardo, D., Solar, H., Garcia-Alonso, A., & Berenguer, R. (2010). Full passive uhf tag with a temperature sensor suitable for human body temperature monitoring. *IEEE Transactions on Circuits and Systems II: Express Briefs*, *57*(2), 95–99.
- Virtanen, J., Ukkonen, L., Bjorninen, T., Elsherbeni, A. Z., & Sydänheimo, L. (2011). Inkjet-printed humidity sensor for passive uhf rfid systems. *IEEE Transactions on Instrumentation and Measurement*, *60*(8), 2768–2777.
- Virtanen, J., Ukkonen, L., Björninen, T., & Sydänheimo, L. (2010). Printed humidity sensor for uhf rfid systems. In *Sensors applications symposium (sas), 2010 ieee* (pp. 269–272).
- Want, R. (2006). An introduction to rfid technology. *Pervasive Computing, IEEE*, *5*(1), 25–33.
- Warnagiris, T. J. (2000). Liquid sensing at radio frequencies. *MICROWAVE JOURNAL-EUROGLOBAL EDITION-*, *43*(9), 140–151.
- Warren, J., Root, P. J., et al. (1963). The behavior of naturally fractured reservoirs. *Society of Petroleum Engineers Journal*, *3*(03), 245–255.
- Wille, S., Buggert, M., Mokrushina, L., Arlt, W., & Smirnova, I. (2010). Effect of electrolytes on octanol-water partition coefficients: Calculations with cosmo-rs. *Chemical Engineering & Technology*, *33*(7), 1075–1082.
- Wohlfarth, C. (2008). *Static dielectric constants of pure liquids and binary liquid mixtures: Supplement to iv/6* (Vol. 17). Springer Science & Business Media.
- Wyman Jr, J. (1933). Dielectric constants: ethanol-diethyl ether and urea-water solutions between 0 and 50. *Journal of the American Chemical Society*, *55*(10), 4116–4121.
- Yeoman, M., Reddy, B., Bowles, H., Zilla, P., Bezuidenhout, D., & Franz, T. (2009). The use of finite element methods and genetic algorithms in search of an optimal fabric reinforced porous graft system. *Annals of biomedical engineering*, *37*(11), 2266–2287.
- Zhang, L., & Wang, Z. (2006). Integration of rfid into wireless sensor networks: architectures, opportunities and challenging problems. In *Grid and cooperative computing workshops, 2006. gccw'06. fifth international conference on* (pp. 463–469).
- Zhou, X., Morrow, N. R., Ma, S., et al. (2000). Interrelationship of wettability, initial water saturation, aging time, and oil recovery by spontaneous imbibition and waterflooding. *SPE Journal*, *5*(02), 199–207.